J|A|C|S
ARTICLES

Published on Web 07/02/2009

Investigation of the Physicochemical Changes Preceding Zeolite Nucleation in a Sodium-Rich Aluminosilicate Gel

Lama Itani,[†] Yong Liu,[‡] Weiping Zhang,*[,‡] Krassimir N. Bozhilov,[§] Luc Delmotte,[†]
and Valentin Valtchev*[,||]

Institut de Science des Matériaux de Mulhouse, LRC 7228 CNRS, Université de Haute Alsace, 3 rue Alfred Werner, 68093 Mulhouse, France, State Key Laboratory of Catalysis, Dalian Institute of Chemical Physics, Chinese Academy of Sciences, 457 Zhongshan Road, Dalian 116023, China, Central Facility for Advanced Microscopy and Microanalysis, University of California, Riverside, California 92521, and Laboratoire Catalyse et Spectrochimie, ENSICAEN, Université de Caen, CNRS, 6 boulevard du Maréchal Juin, 14050 Caen, France

Received March 17, 2009; E-mail: valtchev@ensicaen.fr

Abstract: All industrially available zeolites are obtained from hydrogel systems. Unfortunately the level of understanding of the events preceding zeolite crystallization is far from satisfactory. In this respect, revealing the nature of the processes taking place in the precursor gel is of paramount importance to understanding zeolite nucleation. The investigation of the gel structure, however, is a difficult task due to the complexity of the object in terms of both composition and topology. Therefore, a combination of hyperpolarized (HP) ^{129}Xe NMR−N_2 adsorption−high-resolution transmission electron microscopy−energy-dispersive spectrometry methods complemented by X-ray diffraction, infrared spectroscopy, scanning electron microscopy, and chemical analyses has been employed to study the changes in composition and structure of sodium hydroxide rich aluminosilicate gel yielding zeolite A. The role of each component in the system and the entire sequence of events during the induction, nucleation, and crystallization stages have been revealed. The high concentration of sodium hydroxide in the studied system has been found to control the size and structure of the gel particles in the beginning stage. During the initial polymerization of aluminosilicate species a significant part of the sodium hydroxide is expelled from the gel into the solution, which restricts extensive polymerization and leads to formation of small aluminosilicate particles with open pore structure. The induction period that follows is marked by incorporation of Na back in the bulk gel. The combined action of the Na ion as a structure-directing agent and the hydroxyl group as a mobilizer results in partial depolymerization of the gel and formation of voids with mesopore sizes. The nucleation maximum coincides temporally with development of pores with sizes in the range of 2−5 nm. The amorphous gel undergoes into crystalline zeolite only after these pores have disappeared and the chemistry of the gel has evolved to reach the stoichiometric zeolite composition. It was established unambiguously by high-resolution transmission electron microscopy and HP ^{129}Xe NMR that the nucleation of zeolite occurs in the solid part of the system and the succeeding crystallization commences only after the nuclei are released into the liquid, which is consistent with the autocatalytic mechanism. Also this investigation has demonstrated the unrivaled sensitivity of HP ^{129}Xe NMR that is capable of identifying presence of small amounts of crystalline zeolite material in amorphous medium with detection limit extending below 1 wt %.

Introduction

Zeolites are an important class of industrial materials with steadily growing application in different areas of the chemical industry.[1,2] These microporous crystalline solids have been produced in industrial scale for many years, and both academic and industrial researchers have studied extensively their formation. Nevertheless, there are still a number of questions related to the steps governing zeolite crystallization that remain to be answered. Among them the mechanism of nucleation, which differs from the classical theory describing the nucleation of salts in supersaturated solutions, seems to be the most elusive one.[3−15] The current discussion is not aimed at the generally accepted scheme of zeolite formation around templating species,

---

[†] Université de Haute Alsace.

[‡] Dalian Institute of Chemical Physics.

[§] University of California, Riverside.

[||] Université de Caen.

(1) Davis, M. E. *Nature* **2002**, *417*, 813–821.
(2) Tsapatsis, M. *AIChE J.* **2002**, *48*, 654–660.
(3) Schüth, F. *Cur. Opin. Solid State Mater. Sci.* **2001**, *5*, 389–395.
(4) Tosheva, L.; Mihailova, B.; Wee, L. H.; Gasharova, B.; Garbev, K.; Doyle, A. M. *Angew. Chem., Int. Ed.* **2008**, *47*, 8650–8653.
(5) Barrer, R. M. *Hydrothermal Chemistry of Zeolites*; Academic Press: London, 1992.
(6) Breck, D. *Zeolite Molecular Sieves*; John and Sons: New York, 1974.
(7) Serrano, D. P.; Van Grieken, R. *J. Mater. Chem.* **2001**, *11*, 2391–2407.
(8) Szostak, R. *Handbook of Molecular Sieves*; Van Nostrand Reinhold: New York, 1992.
(9) Thompson, R. W. *Molecular Sieve*; Springer-Verlag: Berlin, 1998; Vol. 1, Chapter 1, pp 1−33.
(10) Cundy, C. S.; Cox, P. A. *Microporous Mesoporous Mater.* **2005**, *82*, 1–78.

10.1021/ja902088f CCC: $40.75

that is, alkali metal cation−water complexes or organic molecules.[16,17] The uncertainties about zeolite nucleation concerns, namely, the spatial and temporal location of the first nuclei as well as the nature and identity of the species involved in their formation. In general, the reaction media yielding zeolite is inhomogeneous, and thus zeolite nucleation involves numerous simultaneous equilibria and condensation steps, which make the above task particularly difficult.[18] Besides the complexity of the process a serious obstacle in its detailed understanding is the large variety of initial systems employed in zeolite crystallization. There are already over 180 zeolite structure types[19] which differ in composition and framework features, and their syntheses require vast variety of chemical precursors. Such diversity in initial composition is due to the fact that "all the intelligence must be contained" in the initial gel in order to obtain a desired zeolite, as stated by Corma and Davis.[20] Consequently, the specifics of each system makes it difficult to establish general crystallization steps that would be common to all zeolite types.

The zeolite-yielding system could be subdivided into two main groups: (i) hydrogel systems comprising bulk solid and liquid parts and (ii) "clear solutions" that contain only discrete gel particles. The latter system has been found to be quite suitable to study zeolite crystallization. Contrary to the conventional gel systems, where a large diversity of (alumino)silicate species is observed, the initially clear solutions contain a limited number of well-defined discrete amorphous precursor particles.[21−24] Hence, interpretation of the results in such systems is simplified and the chances for ambiguous conclusions are reduced significantly. The simplicity of such system and in particular the one yielding silicalite-1 (MFI-type) has attracted a lot of attention in attempts to shed light on zeolite nucleation. Schoeman and Regev were the first to reveal the homogeneous nature of tetraethylorthosilicate-based synthesis of silicalite-1, which contains ca. 84 wt % of the silica in the form of polymeric species with an average particle size of 2.8 nm.[25] Following this method significant contributions to understanding the nucleation of zeolite-type materials at the molecular level have been made by numerous groups employing similar all-silica systems and using different combinations of analytical methods. Recently Rimer et al. provided a relatively comprehensive picture of the template−silica interactions and their further crystallization into an all-silica zeolitic material.[26] A significant step forward among the latest achievements is the determination of the species participating in zeolite growth.[27] A clear solution containing discrete gel particles allowed the birth of the first zeolite crystals to be visualized applying transmission electron microscopy.[28]

The events preceding zeolite nucleation in sodium-rich aluminosilicate hydrogel precursors are even less known. In this respect, understanding of the processes taking place in zeolite-yielding gel-rich systems has lagged behind the knowledge about their highly diluted counterparts, which involve limited number of species. The complexity of the hydrogel systems and their inhomogeneity in both solid and liquid parts makes these precursors particularly difficult to study. It is not surprising that such complexity has kept many researchers away from this topic, and consequently the number of studies devoted to clear precursor systems has been much higher during the past decade. On the other hand, all industrially available zeolites are obtained from hydrogel systems. It is worth recalling that dense hydrogel systems are the precursors for almost all zeolite framework types discovered lately. Therefore, closing the gap in understanding the events preceding zeolite nucleation is of paramount importance for advancement of zeolite synthesis. In this respect, modeling the processes in such systems can be helpful.[29−33]

Despite the overall unsatisfactory level of knowledge in this field, important steps forward have been made recently. For example, an important progress in this field has been the development of a hybrid rheological model describing the thixotropic behavior of particulate suspensions during zeolite crystallization.[34] Also applying transmission electron microscopy several attempts to track down the entire sequence of events leading to zeolite nucleation have been published already.[35−38] Advances in determining zeolite precursor species were recently made by Okubo and co-workers employing high-energy X-ray diffraction technique[39] and a combination of small- and wide-angle X-ray scattering.[40] Very recently Morsli et al. have studied

---

(11) De Moor, P. P. E. A.; Beelen, T. P. M.; Van Santen, R. A.; Beck, L. W.; Davis, M. E. *J. Phys. Chem. B* **2000**, *104*, 7600–7611.

(12) Kirschhock, C. E. A.; Ravishankar, R.; Jacobs, P. A.; Martens, J. A. *J. Phys. Chem. B* **1999**, *103*, 11021–11027.

(13) Watson, J. N.; Iton, L. E.; Keir, R. I.; Thomas, J. C.; Dowling, T. L.; White, J. W. *J. Phys. Chem. B* **1997**, *101*, 10094–10104.

(14) Nikolakis, V. *Microporous Mesoporous Mater.* **2006**, *93*, 101–110.

(15) Tokay, B.; Somer, M.; Erdem-Senatalar, A.; Schüth, F.; Thompson, R. W. *Microporous Mesoporous Mater.* **2009**, *118*, 143–151.

(16) Burkett, S. L.; Davis, M. E. *J. Phys. Chem.* **1994**, *98*, 4647–4653.

(17) Epping, J. D.; Chmelka, B. F. *Curr. Opin. Colloid Interface Sci.* **2006**, *11*, 81–117.

(18) Subotić, B.; Bronić, J.; Jelić, T. A. Theoretical and Practical Aspects of Zeolite Nucleation. In *Ordered Porous Solids: Recent Advances and Perspectives*; Valtchev, V., Mintova, S., Tsapatsis, M., Eds.; Elsevier: Amsterdam, 2008; Chapter 6, pp 127−185.

(19) International Zeolite Association. Database of Zeolite Structures. http://www.iza-structure.org/databases/.

(20) Corma, A.; Davis, M. E. *ChemPhysChem* **2004**, *5*, 304–313.

(21) Kragten, D. D.; Fedeyko, J. M.; Sawant, K. R.; Rimer, J. D.; Vlachos, D. G.; Lobo, R. F.; Tsapatsis, M. *J. Phys. Chem. B* **2003**, *107*, 10006–10016.

(22) Burkett, S. L.; Davis, M. E. *Chem. Mater.* **1995**, *7*, 1639–1650.

(23) Dokter, W. H.; Van Garderen, H. F.; Beelen, T. P. M.; Van Santen, R. A.; Bras, W. *Angew. Chem., Int. Ed.* **1995**, *34*, 73–75.

(24) Schoeman, B. J.; Sterte, J.; Otterstedt, J. E. *Zeolites and Microporous Cryst.* **1994**, *83*, 49–56.

(25) Schoeman, B. J.; Regev, O. *Zeolites* **1996**, *17*, 447–456.

(26) Rimer, J. D.; Fedeyko, J. M.; Vlachos, D. G.; Lobo, R. F. *Chem.—Eur. J.* **2006**, *12*, 2926–2934.

(27) Pelster, S. A.; Kalamajka, R.; Schrader, W.; Schüth, F. *Angew. Chem., Int. Ed.* **2007**, *46*, 2299–2302.

(28) Mintova, S.; Olson, N. H.; Valtchev, V.; Bein, T. *Science* **1999**, *283*, 958–960.

(29) Lechert, H. *Zeolites* **1996**, *17*, 473–482.

(30) Golemme, G.; Nastro, A.; Nagy, J. B.; Subotić, B.; Crea, F.; Aiello, R. *Zeolites* **1991**, *11*, 777–783.

(31) Nikolakis, V.; Vlacho, D. G.; Tsapatsis, M. *Microporous Mesoporous Mater.* **1998**, *21*, 337–346.

(32) Sheikh, A. Y.; Jones, A. G.; Graham, P. *Zeolites* **1996**, *16*, 164–172.

(33) Thompson, R. W.; Dyer, A. *Zeolites* **1985**, *5*, 202–210.

(34) Song, H.; Ilegbusi, O. J.; Sacco, A., Jr. *J. Colloid Interface Sci.* **2006**, *295*, 562–568.

(35) Valtchev, V. P.; Bozhilov, K. N. *J. Phys. Chem. B* **2004**, *108*, 15587–15598.

(36) Valtchev, V. P.; Bozhilov, K. N. *J. Am. Chem. Soc.* **2005**, *127*, 16171–16177.

(37) Tsapatsis, M.; Lovallo, M.; Davis, M. E. *Microporous Mater.* **1996**, *5*, 381–388.

(38) Liang, D.; Follens, L. R. A.; Aerts, A.; Martens, J. A.; Tendeloo, G. V.; Kirschhock, C. E. A. *J. Phys. Chem. C* **2007**, *111*, 14283–14285.

(39) Wakihara, T.; Kohara, S.; Sankar, G.; Saito, S.; Sanchez-Sanchez, M.; Overwag, A. R.; Fan, W.; Ogura, M.; Okubo, T. *Phys. Chem. Chem. Phys.* **2006**, *8*, 224–227.

(40) Wei, F.; Ogura, M.; Sankar, G.; Okubo, T. *Chem. Mater.* **2007**, *19*, 1906–1917.

the microporosity of mordenite precursor gels.[41] Supercritical CO_2 drying was used in that study to retain the structure of the parent gel since the conventional drying led to pore shrinkage due to capillary pressure.

Thus, theoretical models and experimental studies have proved unambiguously the importance of the gel structure for zeolite nucleation. The investigation of the gel structure, however, is a difficult task due to the complexity of the object in terms of both chemistry and morphology. Therefore, there is not a single method of investigation capable of providing all the information necessary for revealing the true nature of the nanoscale events related to zeolite nucleation. Only application of a complex approach that utilizes properly assembled set of complementary methods could provide the desired information.

In this study we conducted synthesis and characterization experiments designed to reveal the changes in the gel texture leading to the nucleation stage in a model system yielding zeolite Na-A. The solid was subjected to conventional drying, and thus only pores supported by a framework sufficiently stable to withstand the capillary pressure were retained. Combination of laser hyperpolarized (HP) ^{129}Xe NMR, N_2 adsorption, high-resolution transmission electron microscopy (HRTEM), and energy-dispersive spectrometry (EDS) analysis, further complemented by conventional methods traditionally used in zeolite investigation, were employed to achieve the above goal.

Experimental Section

Sample Preparation. A silica source (14% NaOH, 27% SiO_2, Fluka) containing low-mass silica species was used and further depolymerized by adding sodium hydroxide (97%, Aldrich) so as to obtain a completely transparent initial solution. The latter was mixed with a clear solution containing sodium aluminate (53% Al_2O_3, 42% Na_2O, Riedel de Haën) and sodium hydroxide (97%, Aldrich). Distilled water was used for both preparation of the initial gels and washing the solid after hydrothermal treatment. The zeolite precursor mixture was produced by vigorous mixing of the alkaline, silicate, and aluminate solutions, where all components were expected to be relatively homogeneously distributed. The composition of the gel was as follows: $6Na_2O/0.505Al_2O_3/1.0SiO_2/150H_2O$. The initial mixture was stirred for 1.0 h at room temperature, and a sample denoted NaA-0 was taken. The remaining gel was then transferred in polypropylene bottles and heated in oven at 90 °C for 30 (NaA-30), 60 (NaA-60), 90 (NaA-90), 120 (NaA-120), 150 (NaA-150), 180 (NaA-180), 210 (NaA-210), 240 (NaA-240), and 300 (NaA-300) min. Solid products were recovered from each treatment by suction filtration using a 0.1 μm filter (Bioblock).

Sodium−calcium ion exchange was carried by mixing 0.5 M $Ca(NO_3)_2$ solution with the solids obtained during the investigation of zeolite crystal growth kinetics in mass ratio 50:1. The exchange was performed at 60 °C. The procedure was repeated four times. After the final exchange the solid was thoroughly washed with distilled water.

In order to compare the gel structure of Na-A precursors with similar zeolite systems a series of gels, yielding Na-P (GIS-type), K-L (LTL-type), and Na-ZSM-5 (MFI-type), were synthesized from gels with the following compositions: zeolite P, $0.9Na_2O/0.1Al_2O_3/1.0SiO_2/80H_2O$; zeolite L, $0.25K_2O/0.08Al_2O_3/1.0SiO_2/10H_2O$; ZSM-5, $0.28Na_2O/0.035Al_2O_3/1.0SiO_2/67H_2O$.

The crystal growth kinetics of zeolite P, zeolite L, and ZSM-5 were studied at 100, 170, and 150 °C, respectively. The obtained solids were recovered as described above.

Characterization. Powder X-ray diffractograms (XRD) were obtained in a PANalytical X'pert Pro diffractometer with fixed slits using Cu/Kα radiation ($\lambda = 1.5418$ Å) with $\theta-2\theta$ mounting. Before analysis samples were finely ground and pressed in a stainless steel sample holder. Spectra were registered in 2θ range of 3−50° with scanning step of 0.1° s^{-1}.

Infrared (IR) spectroscopic analyses were carried out on samples pressed in KBr (in a mass ratio of 1/10) with a Bruker IFS-66 spectrometer in the range of 400−4000 cm^{-1}. The elemental analyses of the solids were performed in an X-ray fluorescence (XRF) spectrometer MagiX (Philips). Prior to the analysis the powdery sample was melted with $Li_2B_4O_7$ at 1300 °C. The resultant glass bead was analyzed under vacuum with a rhodium anticathode (2.4 kW). The mother liquor separated from the solid by high-speed centrifugation was analyzed by atomic absorption spectroscopy (AAS) (Varian Techtron AA6).

Nitrogen adsorption measurements were performed with a Micromeritics ASAP2040 surface area analyzer after being degassed at 90 °C for 1 h and 300 °C for 15 h. Nitrogen measurements were performed on Na and Ca forms of obtained solids. The following conditions were used: equilibrium interval 20 s, equilibrium delay from 20 to 320 min, and relative pressure tolerance 0.01%. It is important to note that nitrogen adsorption in micropores begins at relative pressure of 10^{-7}. DFT pore size analysis was performed with Micromeritics ASAP2040 software. Slit shape pore model was employed, which we consider more appropriate to study the mesopores in zeolite precursor gel. N_2 adsorption measurements were complemented by HP ^{129}Xe NMR in order to obtain a more detailed picture of the pore evolution during hydrothermal treatment of the system. Prior to the measurements the samples were pressed at 8 MPa to reduce the interparticle voids, crushed, and sieved into 20−40 mesh particles. Samples were subjected to dehydration in vacuum ($<10^{-5}$ Torr) for ca. 10−15 h. Optical polarization of xenon was achieved with an apparatus as reported in a previous study,[42,43] with the optical pumping cell in the fringe field of the spectrometer magnet and 60 W diode laser array (Coherent FAP-System).[44,45] A flow of 1% Xe−1% N_2−98% He gas mixture was delivered at the rate of 200−250 mL/min to the sample in the detection region via plastic tubing. Variable-temperature HP ^{129}Xe NMR measurements were performed in the range of 153−293 K. All spectra were acquired on a Varian Infinityplus-400 NMR spectrometer at a frequency of 110 MHz with a $\pi/2$ pulse of 3.0 μs and 2 s recycle delay. Spectra with high sensitivity and good signal/noise ratio have been obtained after 100−200 scans accumulation. The chemical shifts were referenced to the signal of xenon gas. Although the line of the xenon gas is temperature-dependent, generally chemical shifts vary no more than 1 ppm in the temperature range of the experiments.

The structural evolution of the gel was followed by HRTEM. Analyses were performed at room temperature in low-dose mode at 300 kV accelerating voltage in an FEI-Philips CM300 TEM, equipped with LaB_6 cathode, and EDAX energy-dispersive X-ray spectrometer (EDS). A suspension in distilled water was prepared from the solid powder samples without any grinding. After ultrasonication to break up large aggregates a droplet of the suspension was deposited onto holey carbon coated Cu grids. EDS analyses were performed in Nanoprobe mode with beam diameter of 20−200 nm. Scanning electron microscope (SEM) micrographs were taken with a Philips XL30-FEG instrument.

Results

General Characterization. Any physical method of analysis has limits imposed by (i) the size and (ii) the mass fraction of

---

(41) Morsli, A.; Driole, M. F.; Cacciaguerra, T.; Arletti, R.; Chiche, B.; Hamidi, F.; Bengueddach, A.; Quignard, F.; Di Renzo, F. *Microporous Mesoporous Mater.* **2007**, *104*, 209–216.

(42) Zhang, W. P.; Ratcliffe, C. I.; Moudrakovski, I. L.; Mou, C. Y.; Ripmeester, J. A. *Anal. Chem.* **2005**, *77*, 3379–3382.

(43) Moudrakovski, I. L.; Nossov, A.; Lang, S.; Breeze, S. R.; Ratcliffe, C. I.; Simard, B.; Santyr, G.; Ripmeester, J. A. *Chem. Mater.* **2000**, *12*, 1181–1183.

(44) Liu, Y.; Zhang, W. P.; Xie, S. J.; Xu, L. Y.; Han, X. W.; Bao, X. H. *J. Phys. Chem. B* **2008**, *112*, 1226–1231.

(45) Liu, Y.; Zhang, W. P.; Liu, Z. C.; Xu, S. T.; Wang, Y. D.; Xie, Z. K.; Han, X. W.; Bao, X. H. *J. Phys. Chem. C* **2008**, *112*, 15375–15381.

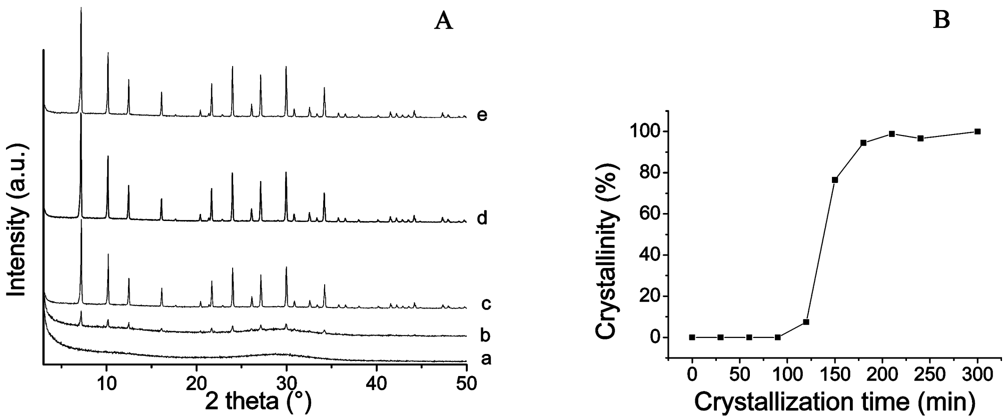

Figure 1. (A) XRD patterns of solids obtained at 90 °C for (a) 90, (b) 120, (c) 150, (d) 210, and (e) 300 min of hydrothermal treatment. (B) Crystal growth kinetics of zeolite A according to the XRD analysis.

the solid phase of interest. Thus, the investigation of early stages of zeolite formation requires appropriate methods combining high sensitivity to crystalline species of limited size with high sensitivity to negligible mass in respect to amorphous matrix.

Conventional XRD analysis is usually employed to study the long-range order of crystalline solids. In other words, the method is not appropriate to study organized structures with size below several unit cells. The detection limit of XRD analysis varies depending on the experimental conditions and the nature of the material under investigation. In general, the detection limit can hardly reach a mass fraction below 3 wt % of the total mass. In the present investigation XRD analysis did not detect crystalline material during the first 90 min of hydrothermal treatment. The first crystalline particles detected by XRD were recorded in the sample subjected to 120 min of crystallization (Figure 1A). Employing highly crystalline zeolite A sample as a reference the zeolite content is evaluated to be about 7 wt %. According to the XRD analysis the crystallization of the amorphous gel into zeolite takes place in the interval from 120 to 150 min. After 150 min of synthesis the crystallinity is 80%, and after 210 min the zeolite content is already 100% (Figure 1B), which is corroborated by the fact that extension of the synthesis time up to 300 min does not improve the X-ray crystallinity of the product.

The series of samples studied by XRD analysis was further examined by IR spectroscopy, thus completing the information of the long-range order (XRD) with short-range order (IR) analysis. The band at 560 cm^{-1} that can be associated with the D4 ring, the dominating secondary building unit in the LTA-type structure, was employed to evaluate the crystallinity of the material.[8,46] This band is not observed in the samples obtained between 30 and 90 min. In the spectrum from the 90 min experiment a weak broad band between 510 and 650 cm^{-1} is present, which might represent nanosized partially ordered particles revealing a similarity with the FTIR results reported by Kosanović et al.[46] The band indicative for D4 ring units can be observed clearly after 120 min of hydrothermal treatment of the solid (Supporting Information Figure 1e), which is in good agreement with the XRD results. According to the IR study the crystallization of the amorphous gel into zeolite A crystals takes place in the time interval from 150 to 210 min. The intensity increase of the 560 cm^{-1} peak is accompanied by a decrease in intensity of the 850 cm^{-1} band that can be assigned to Si−OH bending vibrations. The gradual disappearance of the latter band is consistent with an increase in the number of framework atoms connected via oxygen bridges, which is a further evidence of transformation of the amorphous material into zeolite crystals.[36] Substantial decrease of this band was observed in 120−150 min time laps, which is a strong indication for the beginning of the crystallization process.

SEM inspection of the solid does not show differences in the morphology and appearance of the amorphous particles obtained after different periods of hydrothermal treatment (Supporting Information Figure 2A−D). A few, but relatively large (0.5−1 μm), crystals can be found in the 120 min sample (Supporting Information Figure 2E). The number of the crystals increases with time, and after 210 min particles with amorphous appearance are not observed. After 300 min of hydrothermal treatment well-shaped cubic crystals with edge length of about 1.5−2 μm are formed (Supporting Information Figure 2F). At this stage the crystal size distribution is very narrow, and the fraction of smaller crystallites and aggregates in the solid is negligible.

Bulk chemical analyses of the solid part of the system by XRF show that after mixing the initial reactants the Si/Al ratio is higher than that of a conventional LTA-type material. After 30 min of treatment this ratio is 1.04, and after 60 min of treatment it reaches the perfect zeolite A composition of 1.0. However, local EDS analyses obtained in the TEM from areas 50−100 nm in diameter reveal that the distribution of silicon and aluminum is far from uniform. For the 60 min sample the Si/Al ratio in the gel particles varies from 1.3 to 2.8. Sodium distribution is even more heterogeneous with Si/Na ratio varying from infinity to essentially zero for particles where only Na and O were detected (most probably sodium hydroxide) (Figure 2, parts A and C). For gel particles subjected to 120 min of hydrothermal treatment the variation of the Si/Al ratio is in the range from 0.96 to 1.3 (Figure 2, parts B and D). Further important features of this gel are the absence of pure NaOH particles and the variation of the Si/Na ratio, which does not drop below 100 and approaches 1 for some particles. To complete the analysis of the system the composition of the supernatant was studied by AAS. Variation in the Na, Al, and Si content is observed in the beginning stages of the crystallization process. During the 60 and 90 min hydrothermal treatment periods striking changes in the slopes of the concentration versus reaction time curves for Si, Al, and Na are evident

---

(46) Kosanović, C.; Bosnar, S.; Subotić, B.; Svetličić, V.; Mišić, T.; Dražić, G.; Havancsák, K. *Microporous Mesoporous Mater.* **2008**, *110*, 177–185.

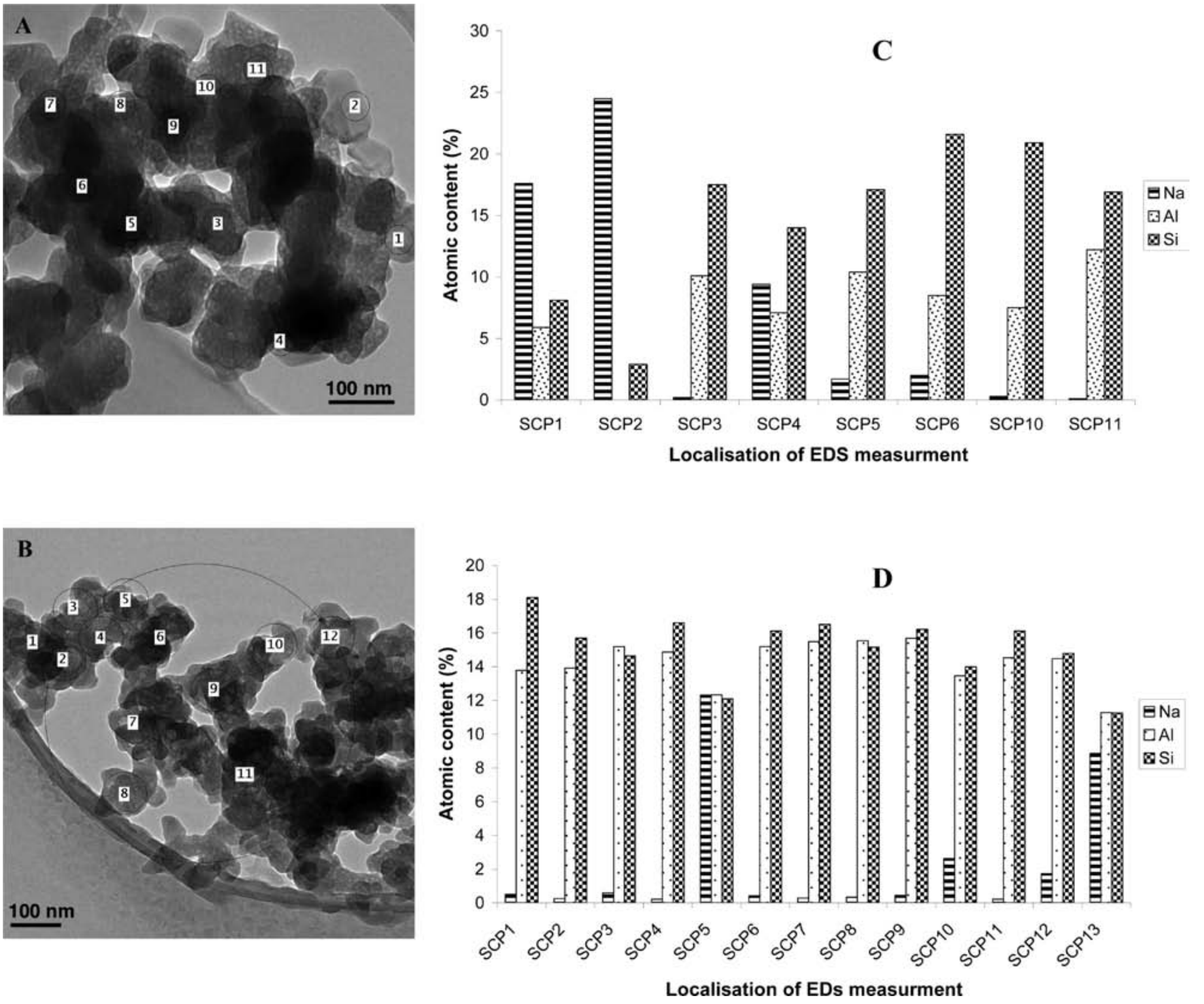

Figure 2. TEM micrograph of solids obtained after (A) 60 and (B) 120 min of hydrothermal treatment with the areas of the EDS analyses. The concentration of Na, Al, and Si in these spots is provided on graphs C and D for 60 and 120 min samples, respectively.

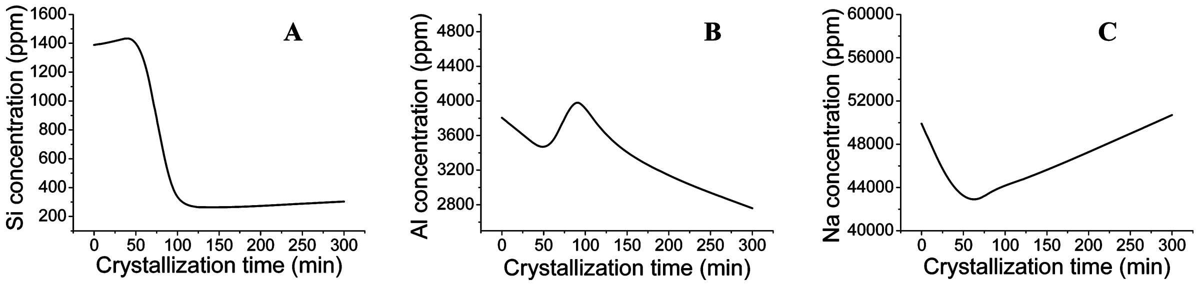

Figure 3. Dissolved silicon (A), aluminum (B), and sodium (C) concentrations of the liquid phase from zeolite A synthesis gels as a function of synthesis time.

(Figure 3), demonstrating that significant transformation in the system takes place at this stage. It is even more illustrative when the changes of Si/Al, Si/Na, and Al/Na ratios in the liquid part of the system are considered (Supporting Information Figure 3). No doubt that the chemical evolution of the system is related with structural reorganization of the solid.[39,40] After the first 90 min the silicon content in the solution becomes almost constant, while aluminum concentration keeps decreasing. After 60 min of treatment in contrast to aluminum the concentration of sodium starts to increase and keeps this trend through the entire remaining course of zeolite crystallization (Figure 3C). This is a consequence of the fact that the initial gel is oversaturated in Na, and once the zeolite framework formation starts the excess Na is expelled in the liquid phase, and furthermore, the overall negative charge of the system is substantially reduced. The above set of experimental data suggests a crystallization scenario where the induction period takes about 90 min, the first crystallites appear after 120 min, and the crystallization of the amorphous into crystalline LTA-type material occurs in the interval of 120−210 min, followed by Ostwald ripening of crystalline particles. As stated earlier the objective of this study is to shed light on the stages preceding

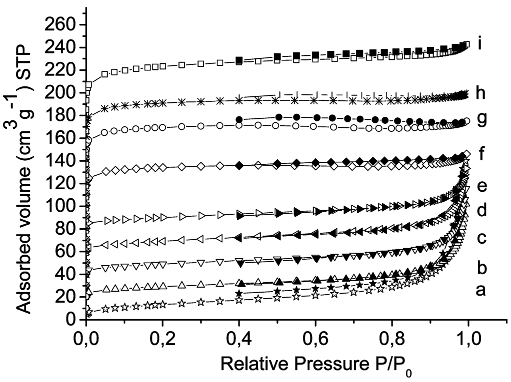

Figure 4. Adsorption/desorption isotherms of the solids obtained after (a) 0, (b) 30, (c) 60, (d) 90, (e) 120, (f) 150, (g) 180, (h) 240, and (i) 300 min of hydrothermal treatment.

the onset of crystallization. Consequently, the physical, structural, and chemical changes in the gel were studied by a combination of N_2 adsorption, HP ^{129}Xe NMR, and HR TEM.

N_2 Adsorption Study. Nitrogen adsorption measurements were employed to study the external surface area of as-synthesized samples since zeolite A in its sodium form does not adsorb the N_2 molecule. The results of these measurements show a gradual decrease of the specific surface area (S_{BET}) with crystallization time, namely, from 38 $m^2\ g^{-1}$ for the initial gel to 3.5 $m^2\ g^{-1}$ for the highly crystalline sample obtained after 300 min of hydrothermal treatment. The observed decrease (S_{BET}) is obviously a consequence of the formation of larger particles in the course of zeolite crystallization. Along with the specific surface area a decrease of the total pore volume from 0.21 to 0.002 $cm^3\ g^{-1}$ is observed. In this case the total pore volume corresponds to the mesopore volume of the solid. It is worth recalling, however, that the samples were dried under ambient conditions that might destroy pore structures with limited framework stability.

Further, in order to evaluate the contribution of the zeolite part Ca^{2+}-exchanged forms of the solids were subjected to N_2 adsorption measurements. A series of adsorption/desorption isotherms of the samples is shown in Figure 4. The isotherm of the initial gel is close to type III, which is typical of nonporous or macroporous materials. The uptake at high relative pressure with hysteresis is indicative of the generated interparticle mesoporosity. Indeed, the density functional analysis (DFT) of the pore size reveals the presence of mesopores in the range of 20−100 Å. All isotherms of the solids for samples from 30 to 120 min syntheses comprise such uptake and hysteresis loop at high relative pressure. In the time interval from 30 to 120 min the solid contains large amorphous aggregates with distinct mesoporosity, which is not influenced by the drying procedure. No uptake at high relative pressure is observed in the isotherms of materials subjected to longer hydrothermal treatment. These data show that the crystallization from amorphous into crystalline LTA-type material takes place after 120 min of synthesis. At this stage large aggregates containing textural pores disappear. Samples obtained for more than 150 min of hydrothermal treatment show type I isotherms characteristic of microporous zeolite-type materials. The data from adsorption/desorption isotherms of calcium-exchanged samples are summarized in Table 1. A slight increase of S_{BET} coupled with the appearance of micropore volume (0.02 $cm^3\ g^{-1}$) is detected after 120 min of synthesis. After this stage a rapid growth of the specific surface area can be seen, which is due exclusively to the increase in the micropore area. Micropore volume increases also and reaches a value characteristic of highly crystalline LTA-type material. DFT was performed on the N_2 adsorption data in order to obtain a more comprehensive picture of the pore size distribution during different stages of zeolite formation. The pore size classes found throughout the crystallization process are presented in Table 2. Zeolite micropores (0−10 Å) are not present at the beginning of the crystallization process. Pores in the range of 10−20 Å exist in all stages, and their distribution does not show a particular trend. In contrast, the fraction of 20−50 Å pores increases at a steady rate and reaches maximum after 120 min of hydrothermal treatment. It is worth recalling that at this instant the crystallization starts. Further hydrothermal treatment results in complete disappearance of this pore fraction. No substantial fluctuation in the fraction of larger pores (50−100 Å) is apparent during the induction period. The latter do not appear in the samples treated longer than 120 min (Table 2). N_2 adsorption measurements of zeolite Na-A and its calcium-exchanged counterpart provided reasonably detailed information about the pore structure of the solid and its evolution as a function of synthesis time. Although the pore size analysis provides important insights its significance can be understood only if it is associated with specific structural information. In other words, it is necessary to identify the structure and composition of the material, which comprises the matrix, the immediate vicinity, and the interface where the pores develop. This is a particularly challenging task in light of the low abundance of the pore fraction during the stages of emerging zeolite nuclei. In order to accomplish the investigation of the structure of the pore interfaces during zeolite A nucleation we employed laser HP ^{129}Xe NMR, which combines high sensitivity to different pore sizes with low detection limit.

Table 1. N_2 Adsorption Data of Calcium-Exchanged Samples Obtained at 90 °C for Different Periods of Time

sample	S_{BET} ($m^2\ g^{-1}$)	total pore volume ($cm^3\ g^{-1}$)	micropore volume ($cm^3\ g^{-1}$)
0 min[a]	49	0.22	0
30 min	34	0.13	0
60 min	35	0.11	0
90 min	38	0.11	0
120 min	63	0.10	0.02
150 min	387	0.22	0.20
180 min	488	0.27	0.22
240 min	494	0.28	0.25
300 min	646	0.37	0.26

[a] Initial gel not subjected to hydrothermal treatment.

Table 2. Volumetric Contribution of Different Pore Size Classes Throughout the Zeolite Crystallization Process

synthesis time (min)	cumulative pore volume ($cm^3\ g^{-1}$)[a]	pore size classes (%)			
		0−10 Å	10−20 Å	20−50 Å	50−100 Å
0	0.1	5	15	40	40
30	0.012	0	33	42	25
60	0.015	0	20	53	27
90	0.017	0	18	53	29
120	0.02	0	15	55	30
150	0.03	33.3	67	0	0
180	0.08	50	50	0	0
240	0.08	50	50	0	0
300	0.24	92	4.2	4.2	0

[a] Prior to N_2 adsorption measurements Na^+ cations were exchanged by Ca^{2+}.

HP ^{129}Xe NMR Investigation. Previous studies have shown that Xe atoms can penetrate into the pore structure of zeolite

A.[47−50] The α-cage of this zeolite, with size of 1.14 nm, is able to accommodate between one and seven xenon atoms as shown by Chmelka et al.[51] This particular property is employed in the present study to try to detect the appearance of the first nuclei in the system. Variable-temperature HP ^{129}Xe NMR experiments were performed in order to obtain signal with maximum intensity. Namely, decrease in temperature restricts the mobility of Xe atoms, and thus more inert gas atoms can be occluded. Consequently, an increase in intensity of the signal at lower temperatures is observed mainly due to the stronger Xe−Xe interactions.[52] Another feature of variable-temperature HP ^{129}Xe NMR is the shift of Xe peaks to higher ppm values with decrease in temperature. These particularities can be seen in the spectra of the initial gel, where besides the peak of Xe in the gas phase (0 ppm) a peak at 33 ppm is observed at ambient conditions. The decrease of the temperature to 153 K results in a spectacular increase in peak intensity and position shift to 112 ppm (Figure 5A). According to the N_2 adsorption measurements the initial gel contains exclusively mesopores, and consequently the observed peak, denoted peak a, can be attributed to this pore fraction. No changes in the peak position and intensity are observed after 30 min of hydrothermal treatment (Figure 5B). This is actually the time the system reaches the crystallization temperature (90 °C). Changes in the HP ^{129}Xe NMR spectrum are evident after 60 min of crystallization (Figure 5C). In addition to the peak attributed to the mesopores a new one appears at 233 K, which provides indirect information of structural changes in the solid. This second peak was attributed to the birth of the first zeolite entities in the gel. The latter, denoted as peak b, is shifted to 125 ppm with the decrease of the temperature to 153 K. The absence of peak b at room temperature is a sound proof for the extremely low abundance of zeolite phase at this stage. The detection of the zeolite is enhanced at low temperatures due to the stronger interaction of Xe with zeolite structure. The changes of the intensity of peaks a and b are coupled, that is, the increase in intensity of peak b is accompanied by intensity decrease of peak a (Figure 5D). After 120 min of hydrothermal treatment, peak a completely disappears and only peak b is observed in the HP ^{129}Xe NMR of the solid (Figure 5E). The absence of the mesoporous peak in the HP ^{129}Xe NMR spectra of the 120 min sample is fairly surprising considering the data from N_2 adsorption measurements. During this stage the mesoporous fraction is still dominant in the sample. Nevertheless, only the signal from Xe atoms in the zeolite micropores can be observed in the spectra. To understand this phenomenon it is worth recalling that Xe attraction depends on the local electrostatic forces, which are much higher in crystalline microporous material in respect to textural mesopores in an amorphous gel. Thus, Xe is preferentially adsorbed in the zeolite micropores, and when the mass of the zeolite reaches a critical level all xenon atoms are adsorbed in the zeolite part of the solid. The spectra collected from the sample hydrothermally treated for 150 min differs from the previous one (Figure 5F). In addition to peak b a new peak c appears in the spectrum. The increase of the intensity of the latter is coupled with the appearance of a new peak denoted d after 180 min of hydrothermal treatment. Peaks c and d are clearly observed at 173 K (Figure 5G). With decrease in temperature to 153 K their positions shift to 148 and 229 ppm, respectively (Figure 5H). The spectra from samples obtained after more than 180 min of hydrothermal treatment, including the highly crystalline LTA-type material synthesized for 300 min (Figure 5H), comprised the peaks b, c, and d (Figure 5), which were tentatively assigned to Xe_2, Xe_7, and Xe_3 atoms in the α-cage of zeolite A.[53−55] The sodium cations may hinder the Xe atoms mobility and cause such a heterogeneous distribution of adsorbed Xe atoms in zeolite A. It is worth recalling that the xenon signal is influenced by the local pattern of distribution and configuration of electrostatic charges in the zeolite pore system. Thus, the xenon interactions are strongly influenced by the completion of zeolite crystals and in particular the α-cage, where the probe atoms are situated. Hence, in the nucleation stage, when the number of nonaccomplished zeolite unit cells is high, the distribution of Na cations and consequently the ratio between different xenon signals could be different.

HRTEM Investigation. HRTEM was used as the primary tool for direct observation of the events at nanometer scale. Without such information the results of the above analysis are difficult to interpret since the obtained information is based on the entire system and it is difficult to be related with events of the local level. TEM inspection revealed that the initial gel and the amorphous solids formed during the hydrothermal treatment exhibit globular structure. Close examination showed that gel aggregates are built of randomly connected particles with oval shape and size around 30−50 nm. A characteristic feature of the aggregates is the open dendrite-like structure. Aluminum hydroxide and sodium hydroxide crystals were identified by electron diffraction and EDS analyses in the initial gel, and some of these crystals persist during the induction period as well. These phases form isolated particles separated from the amorphous part of the system. Their formation is metastable, and they disappear after 60 min of hydrothermal treatment. Another characteristic feature of the solid part of the zeolite-yielding gel is its heterogeneous structure, which has been observed already in sodium-rich aluminosilicate gels.[35,36] Small round granule-like areas, several nanometers in size, are present inside the gel particles. They appear as bright spots on the generally darker background of the gel matrix. A few of these granule-like areas are observed in the initial gel (Figure 6A). Their number and size increase with crystallization time, and after 120 min of treatment a dense network of such granules or pores is present in all gel particles (Figure 6B). Contrast differences in bright field imaging mode suggest that these granules represent either empty pores or cavities formed during gel drying or they consists of material with lower average atomic number, most probably enriched in hydroxyl groups or water molecules as compared to the average gel composition. Prolonged exposure under the electron beam causes these granules to expand until eventually they burst and collapse. From these observations one can infer the possibility that the granules or pores are inclusions rich in volatile components or even liquid phase. The sizes of the granule-like pores detectable by TEM vary from 2 to 5 nm

---

(47) Chen, Q. J.; Fraissard, J. *J. Phys. Chem.* **1992**, *96*, 1814–1819.

(48) Samant, M. G.; De Ménorval, L. C.; Dalla Betta, R. A.; Boudart, M. *J. Phys. Chem.* **1988**, *92*, 3937–3938.

(49) Jameson, C. J.; Lim, H. M.; Jameson, A. K. *Solid State Magn. Reson.* **1997**, *9*, 277–301.

(50) Ripmeester, J. A.; Ratcliffe, C. I. *J. Phys. Chem.* **1990**, *94*, 7652–7656.

(51) Chmelka, B. F.; Raftery, D.; McComick, A. V.; de Menorval, L. C.; Levine, R. D.; Pines, A. *Phys. Rev. Lett.* **1991**, *66*, 580–583.

(52) Springuel-Huet, M. A.; Cuenneau, F.; Gédéon, A.; Corma, A. *J. Phys. Chem. C* **2007**, *111*, 5694–5700.

(53) Li, F. Y.; Berry, R. S. *J. Phys. Chem.* **1995**, *99*, 2459–2468.

(54) Jameson, C. J.; Jameson, A. K.; Gerald, R., II; De Dios, A. C. *J. Chem. Phys.* **1992**, *96*, 1676–1689.

(55) Jameson, C. J.; Jameson, A. K.; Gerald, R., II; De Dios, A. C. *J. Chem. Phys.* **1992**, *96*, 1690–1697.

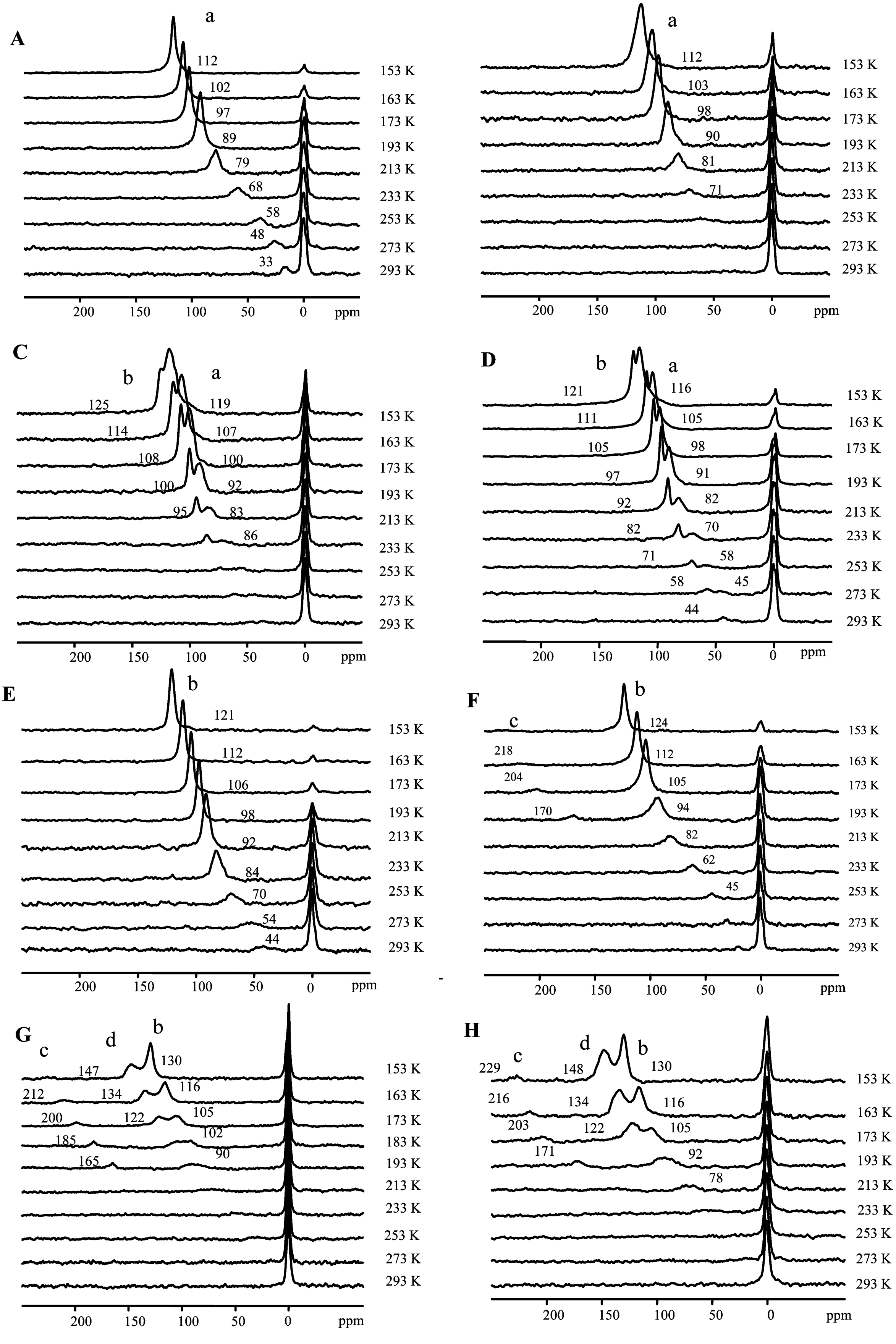

Figure 5. Temperature-dependent HP ^{129}Xe NMR spectra of solids obtained after (A) 0, (B) 30, (C) 60, (D) 90, (E) 120, (F) 150, (G) 180, and (H) 300 min of hydrothermal treatment.

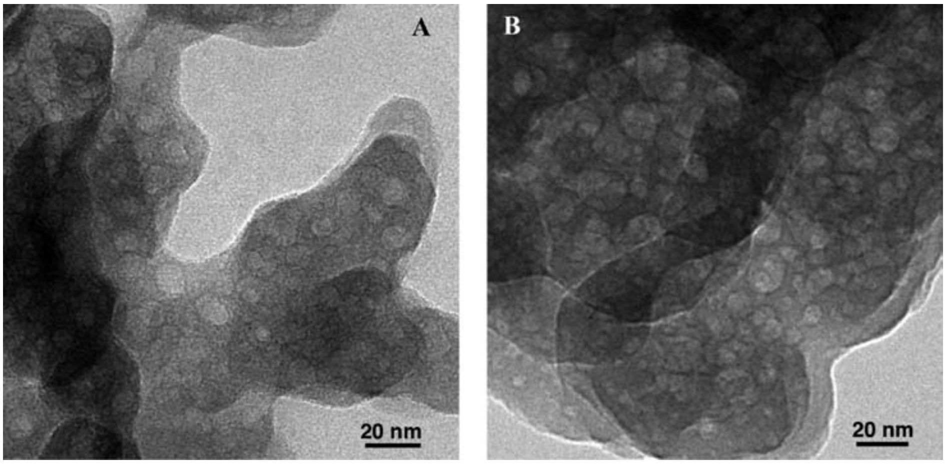

Figure 6. TEM micrographs of gel treated under hydrothermal conditions at 90 °C for (A) 60 and (B) 120 min.

in the beginning of the crystallization process (30−60 min) to 10−15 nm after 120 min of hydrothermal treatment. At this later stage of treatment many of the granules are defined by relatively straight faceted interfaces, which suggests long-range order and crystalline state at a narrow interface region. The presence of a robust outer shell could explain the relative stability of the granule-like pores or inclusions, which are able to withstand the changes in the amorphous network during the drying process. These pores or inclusions in the gel disappear during the main crystallization stage. Thus, the TEM investigation confirmed the results from N_2 adsorption measurements and HP ^{129}Xe NMR analyses that during the induction period the solid part of the system comprises voids with mesopore dimensions.

For the sake of comparison a series of gels, yielding Na-P (GIS-type), K-L (LTL-type), and Na-ZSM-5 (MFI-type), was studied by HRTEM. The content of alkali metal cations is lower compared to zeolite Na-A yielding gel employed in the present investigation. Representative TEM micrographs of the gel structure prior to the crystallization into zeolite are shown in Figure 7. Two major differences between the sodium-rich zeolite A precursor (Figure 7A) and the gels with low alkali metal content (Figure 7B−D) can be observed: (i) the size of the individual gel particles increases with decrease of alkali metal concentration, and (ii) the low alkali content results in glasslike gel structures without voids and intraparticle porosity. The transformation of these gels was followed throughout the entire induction period, and no visible changes in the gel structure were observed. The larger gel particles with smaller solid−liquid interface area in these precursors (Figure 7B−D) are in good correlation with the lower nucleation and crystal growth kinetics of these zeolites with respect to zeolite A. The solid precursor of the latter (Figure 7A) exhibits much more open structure that favors the exchange in the system and accelerates the nucleation rate.

Although not abundant in the gel matrix individual zeolite A crystallites were detected and imaged by HRTEM in the products from the 60 and 120 min treatments (Figure 8). They are about 10−20 nm across and display typical for LTA structure lattice fringes of 12, 8.5, and 5.5 Å which correspond to the (002), (022), and (420) interplanar distances, respectively.

Discussion

Detection and identification of minor amounts of crystalline material in an amorphous matrix depends on the amount and particle size of crystallites, which is a direct consequence of the detection limit of the methods employed. The physical methods employed in this study show substantial differences in detection limit in respect to the presence of LTA-type crystals. Zeolite crystals are clearly identified after 120 min of hydrothermal treatment using XRD, which is confirmed by the SEM inspection of the sample. IR analysis also records the presence of a small amount of zeolite after 120 min of hydrothermal treatment and crystallization during the time interval of 150−210 min. HRTEM data shows the presence of individual isolated LTA crystals already in the 60 min experiment.

Indirect structural information extracted by N_2 adsorption and HP ^{129}Xe NMR suggests the appearance of crystalline zeolite after 60 min as well. In summary, the collected data are in agreement that the system crystallizes within 210 min yielding a pure LTA-type zeolite. However, the direct structural methods did not provide useful information about the events preceding the zeolite crystal growth stage. Valuable information revealing physical and chemical aspects of the changes in the system leading to zeolite nucleation can be extracted by employing methods providing complementary information related to chemical, structural, and textural changes in the precursor system. For instance, the global bulk composition of the initial gel shows that after 30 min of hydrothermal treatment the Si/Al ratio in the system is close to zeolite A composition and after 60 min the solid part of the system has reached already the stoichiometric composition of the crystalline material. The analysis of the liquid part of the system reveals that consequential developments take place between 60 and 90 min of hydrothermal treatment leading to changes in the concentrations of Na, Si, and Al. After this stage no fluctuations in silicon content in the solution are observed. The concentration of aluminum in the solution slowly decreases suggesting higher silicon content in the amorphous solid. The sodium content in the mother liquor gradually increases due to partial release of sodium from the gel as a consequence of both zeolite crystallization and the need for compensation of the negative charge of the amorphous matrix. These results reveal an intensive exchange between the solid and liquid parts of the system.

Local EDS analyses show that the distribution of the structure-directing agent (Na) and the framework constituents (Si and Al) vary substantially in the amorphous part of the system. Sodium hydroxide crystalline particles with morphological features different from the aluminosilicate gel are present in the peripheral parts of the gel aggregates from the starting

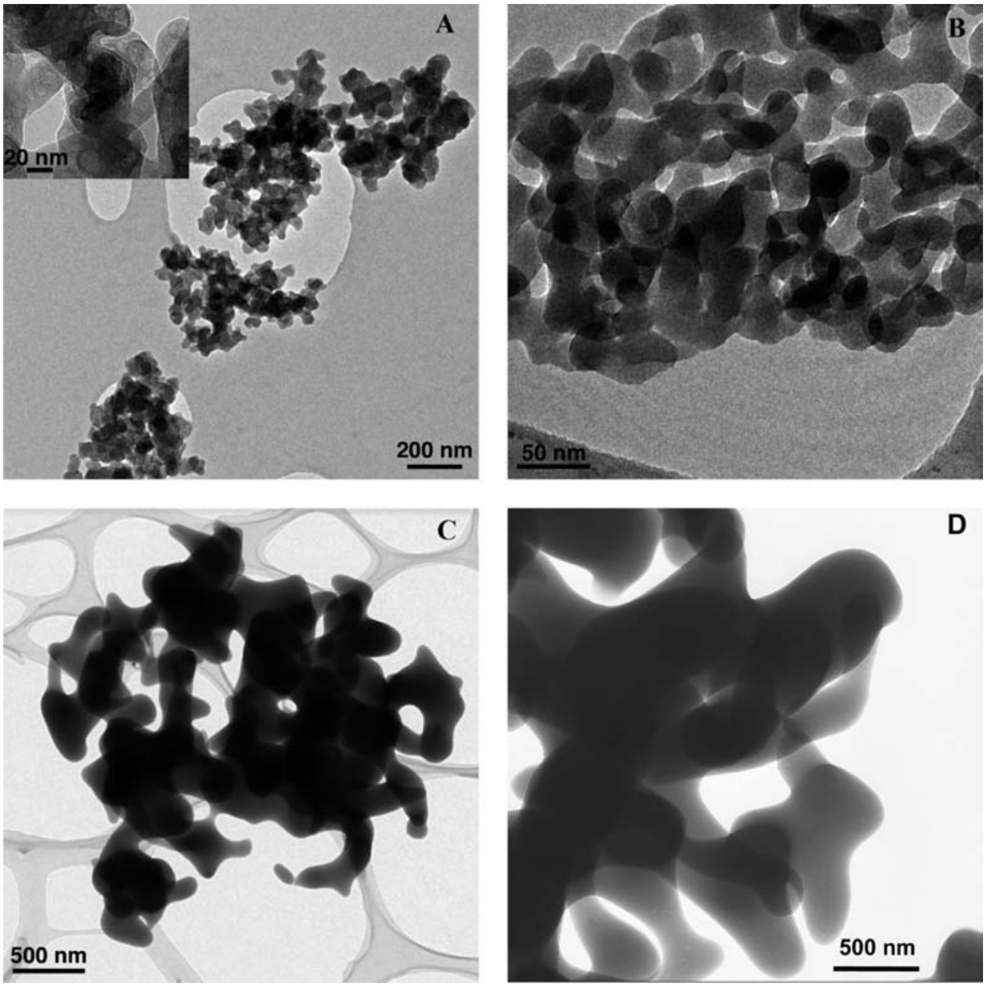

Figure 7. TEM images of amorphous precursors yielding (A) zeolite Na-A from a gel with composition $6Na_2O/0.505Al_2O_3/1.0SiO_2/150H_2O$, (B) zeolite Na-P from a gel with composition $0.9Na_2O/0.1Al_2O_3/1.0SiO_2/80H_2O$, (C) zeolite K-L from a gel with composition $0.25K_2O/0.08Al_2O_3/1.0SiO_2/10H_2O$, and (D) Na-ZSM-5 from a gel with composition $0.28Na_2O/0.035Al_2O_3/1.0SiO_2/67H_2O$. Inset in panel A: high-resolution image of the voids in the gel can be seen.

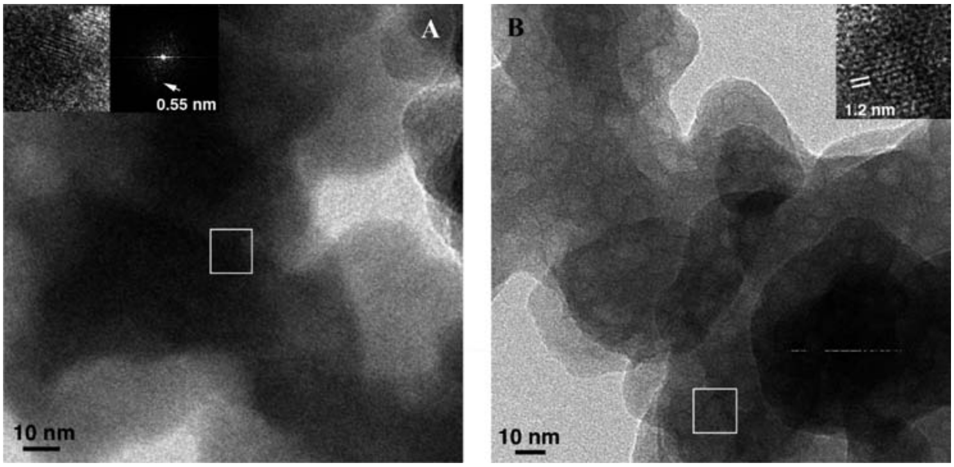

Figure 8. HRTEM images of gel structures obtained after 60 (A) and 120 (B) min of hydrothermal treatment. The insets show magnified views of zeolite A crystallites embedded in gel matrix. The crystal lattice contrast is enhanced by FFT filtering.

mixture as well as in the products from the induction period. It is worth recalling that a great excess of sodium is employed in the system under investigation. Thus, the presence of pure NaOH in the dry product is not surprising. The local chemical analysis reveals a much more important fact, that is, the content of sodium is very low in the bulk gel particles (Figure 2). This finding is of paramount importance to understanding the events during the induction period. During mixing of dissolved silica and alumina sources, sodium-poor aluminosilicate gel is formed. On the other hand, the silicon to aluminum ratio in the gel aggregates varies substantially and deviates from 1:1 ratio, characteristic of Na-A. It is worthwhile to mention that the

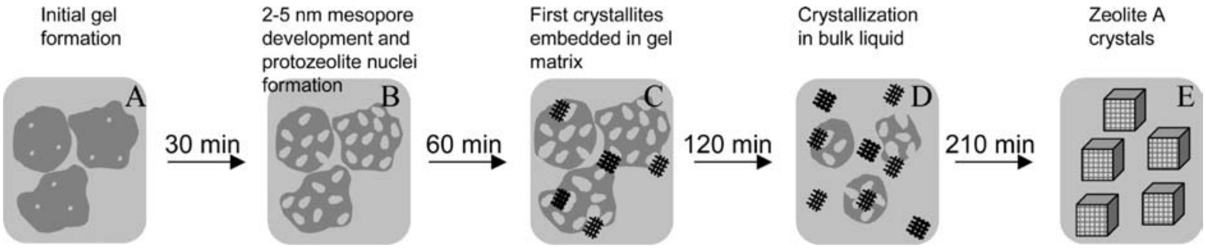

Figure 9. Schematic presentation of most important stages of zeolite A formation from a sodium-rich aluminosilicate system. The important stages of zeolite formation are marked with A, B, C, D, and E, respectively.

deviation from Si/Al = 1 in the gel is much larger in the beginning of the induction period (Si/Al = 1.3−2.8; Figure 2, parts A and C) than in its final stages (Si/Al = 0.97−1.31; Figure 2, parts B and D). Local analyses revealed that the core of gel particles is richer of silicon (see Figure 4 of the Supporting Information), which is in good agreement with the decrease of aluminum content in solution during crystallization stage. In other words, the stoichiometry of zeolite framework (Si/Al = 1) requires the misbalance between silicon and aluminum in the initial gel to be compensated by preferential incorporation of dissolved aluminum species. These results show that during the induction period significant diffusion takes place, which brings the gel composition close to zeolite A stoichiometry, although the solid remains still amorphous. This might be an indication that short-range ordering at the atomic scale is transforming the amorphous precursor into material close to zeolite in chemistry and microstructure, a feature, which is below the detection limit of the available physical methods. The changes in the system, induced by the combined action of structure-directing agent (Na^+) and mobilizer (OH^-), cannot be accomplished without a partial dissolution of the solid and solution-mediated transport of the alumina and silica species. In the present study a large excess of sodium hydroxide and highly reactive silica and alumina sources were employed to ensure supersaturation in the system. Nevertheless, the induction period takes up half of the entire crystallization duration, which is a consequence of the nonhomogeneous distribution of the reactants in the initial gel. It appears that the start of the nucleation process is controlled on one hand by the local supersaturation and on the other by the rate of diffusion in the gel that produces the required critical ratio between zeolite-building components.

As already discussed, local EDS analyses reveal that during polymerization of aluminosilicate species sodium is expelled from the gel. In sodium-rich systems this process leads to increased sodium concentrations in the solution that restrain the polymerization of aluminosilicate species. As a consequence smaller gel particles with much larger dense gel−bulk liquid interface are formed, which has important consequence on the nucleation kinetics. Usually such systems yield highly crystalline zeolite product within several hours. In contrast, much slower crystal growth kinetics is observed in low-alkali systems containing large bulk gel particles.[56] As seen in this study, the comparison of Na-A zeolite with Na-P (GIS-type), K-L (LTL-type), and Na-ZSM-5 (MFI-type) reveals that the precursors in the latter three systems produce larger gel particles with glassy structure, lacking any voids and with smaller solid−liquid interface area (Figure 7). These results are in good correlation with the lower nucleation and crystal growth kinetics of these zeolites with respect to zeolite A. The solid precursor of the latter (Figure 7A) exhibits much more open structure that favors exchange in the system and accelerates nucleation rate.

The results from bulk and local chemical analyses show that during the induction period sodium penetrates inside aluminosilicate species breaking their structure and favoring the exchange with other parts of the system. Thus, the concentration of sodium hydroxide is particularly important for the kinetics of the crystallization process. The most important factors controlling the kinetics of the reaction in the system are (i) the size and morphology of gel particles, (ii) the surface area of the solid−liquid interface, (iii) the rate of dissolution of silica and alumina precursors, and (iv) the ability of the gel to transport zeolite-building species. Another important issue affecting zeolite nucleation, which is difficult to evaluate in a straightforward manner, is the presence of channels and cavities facilitating the transport of dissolved aluminum and silicon species. Hence, understanding the effect of the gel pore structure on zeolite nucleation is probably among the most elusive issues related to zeolite nucleation. The importance of the gel pore structure in zeolite nucleation has been predicted by Nikolakis et al.[31] In a previous study we have identified these cavities by means of TEM and pointed out their importance in the nucleation of zeolite A.[36] In the present investigation a comprehensive analysis of different pore size classes, their development and disappearance in the course of crystallization process was performed by a combined N_2 adsorption−HP ^{129}Xe NMR−HRTEM investigation. In addition, the nucleation in the sodium-rich zeolite A yielding system was compared with the formation of zeolites crystallizing in systems comprising different amounts of alkali cations. A schematic presentation of the changes in the pore structure of gel particles, appearance of nuclei to complete transformation of the solid into zeolite, is presented in Figure 9.

Nitrogen adsorption measurements reveal that prior to the onset of zeolite crystallization substantial changes in gel pore structure take place (Table 2). Among the different pore size classes, determined during the induction period, the one that substantially increases its relative proportion of the total pore volume is the 20−50 Å mesopore class. In contrast to smaller (10−20 Å) pores that vary throughout the crystallization process without showing any specific trend, the fraction of 20−50 Å mesopores steadily grows during the induction period and reaches maximum after 120 min of hydrothermal treatment (Figure 9, parts C and D). After that this pore fraction suddenly disappears and is not observed until the end of the crystallization process. Similarly, larger pores (50−100 Å) are not observed in the samples treated under hydrothermal conditions for more than 120 min. This pore fraction disappears together with the smaller (20−50 Å) mesopores. It is noteworthy that the

---

[56] Valtchev, V.; Bozhilov, K. N. *Book of Abstracts of the 15th International Zeolite Conference*, Beijing, China, August 12−17, 2007; p 162.

disappearance of these two classes of mesopores coincides with the start of the crystallization process (Figure 9D). What is the specific role of mesopores in zeolite nucleation process is a question that cannot be answered equivocally. Certainly, the diffusion of the dissolved species in these mesopores is much more efficient than that in micropores (10−20 Å). The transport of nutrients, even low-weight silica species, will be difficult through the latter. Another aspect would be the capillary pressure in the mesopores that might favor zeolite nucleation. It should be added that the mesopores are large enough to transport fragments of zeolite structure (protozeolite nuclei) to the bulk liquid. According to Nikolakis et al.[31] mesopores with sizes of 50−100 Å are important for zeolite nucleation. In addition to corroborating this conclusion the present study has revealed that smaller mesopores (20−50 Å) also play an important role in the zeolite nucleation process since their development and disappearance coincide with the nucleation and crystal growth stages, respectively.

The presence of mesopores was unambiguously proved by HP ^{129}Xe NMR investigation. Peak a (Figure 5) stems from pores larger than 20 Å, which disappear during crystallization of the amorphous into zeolite. The peak was still distinguishable in the 90 min sample but completely disappeared in the 120 min one (Figure 5). As stated above the stronger electrostatic field of the microporous framework is the reason for preferred Xe adsorption in zeolite pores. On the other hand, the increase in size of the gel cavities with synthesis time (Figure 6B) might be the reason for the weaker interaction with polarized Xe atoms. Consequently, the Xe is adsorbed in zeolite A pore structure, although the mass of zeolite is negligible. Such interpretation is in agreement with the disappearance of peak a (Figure 5), when the mesopore volume is still several times larger than the micropore one. It is interesting to evaluate the quantity of zeolite, which caused the dramatic changes in HP ^{129}Xe NMR spectra. According to the XRD analysis after 120 min of hydrothermal treatment the zeolite content is 7 wt %. This amount is sufficient for all Xe atoms to be incorporated into the microporous material and to hide the presence of mesopores in the sample. Presence of zeolite in the 90 min sample is not detected by the XRD technique, which suggests an amount below 2−3 wt %. Having in mind the low nucleation rate in the early stages and the autocatalytic character of the crystallization process,[57,58] the amount of microporous zeolite-type material after 60 min of hydrothermal treatment is expected to be substantially below 1 wt %. Therefore, it is not surprising that the employed physical methods do not show the presence of LTA-type material in the solid at this stage. The presence of zeolite A is proved unambiguously by the HP ^{129}Xe NMR. This fact demonstrates the exceptional sensitivity of the NMR method for studying zeolite-type materials and for detection of very small amounts of microporous material. It also provides more statistically reliable information due to the bulk character of the studied samples as opposed to the TEM where the statistical significance of any finding is difficult to estimate.

The results of HP ^{129}Xe NMR analysis, namely, the presence of crystalline LTA-type material, are confirmed by HRTEM. Due to low abundance and instability under the electron beam a systematic examination of many sample grids in the TEM was necessary in order to find evidence of the presence of crystalline nuclei during the induction period. Zeolite crystallites embedded in the amorphous matrix were found in the 60 and 120 min hydrothermal treatment experiments, since these two samples were selected for more thorough examination (Figure 8). The presence of crystallites in the gel matrix even after 120 min of treatment appears to be in conflict with the XRD study, which shows 7−8% LTA-type in the solid after 120 min. A plausible explanation of this seeming discrepancy is that nucleation in the gel matrix does not stop abruptly and it is still in progress while earlier formed nuclei are growing in size. Most of the nuclei seem to be released from the gel into the mother liquor, where they develop into larger crystals. Morphologically most of the zeolite A crystals are represented by individual euhedral single crystals (Supporting Information, Figure 3F), which confirms the interpretation of crystal growth in the liquid phase, an environment where contact and interference by other crystals or solids is limited. These observations can be considered in the light of the so-called autocatalytic nucleation,[57,58] where the nuclei become active after being released into the liquid. Owing to the growth of liberated nuclei, the zeolite surface area increases, which accelerates the reaction rate. The revised model of the autocatalytic nucleation postulates that dormant nuclei are located near the surface of the gel particles.[59] However, sodium-rich aluminosilicate gels possess fairly complicated dendrite-like morphology. Our TEM investigation show that the gel is built of very small randomly aggregated particles, which do not form bulk structures. Hence, terms such as internal and outer surface become relative and not very precise. In addition, the impact of the gel pore structure in the exchange between solid and liquid parts of the system is not taken under consideration in the revised autocatalytic nucleation model. For certain systems the contribution of this variable could be important and merits a much closer consideration in the theoretical models.

This study deals with the nucleation in sodium-rich aluminosilicate gel systems. However, there is not a clear-cut boundary between nucleation, crystallization, and growth in general and in zeolite-yielding systems in particular. By definition a crystalline state requires long-range order. A specific critical value for defining a crystalline state is a matter of convention and is yet to be established. In any case for a particular long-range order to qualify for a crystalline state it must be manifested as three-dimensional order of its constituent atoms, ions, and/or molecules in at least several unit cells. The transition from fully amorphous to perfectly crystalline state is gradual. It starts with assembling atoms and ions in specific groups with distinct arrangements also known as short-range order, which later evolve into more complex architectures that develop into well-defined nuclei, which in turn could continue to grow and form macroscopic crystals.

The set of experimental methods employed in the present zeolite study is not directed toward the study of the nature and level of organization during the stage of chemical bonding and short-range order formation as well as identification of the species participating in this process. In contrast the current investigation is focused on the temporal and spatial occurrences of nucleation and crystal growth and the mechanisms these processes are controlled by. Our TEM study of the early stages of the zeolite formation (60−120 min) showed the presence of small crystallites comprising volumes between 4 and 10 unit cells. These zeolite nuclei are deeply embedded in the gel matrix that suggests an autochthon formation. Although not the primary

---

(57) Subotic, B. *Zeolite Synthesis*; ACS Symposium Series No. 398; American Chemical Society: Washington, DC, 1989; pp 110−123.

(58) Subotic, B.; Graovac, A. *Stud. Surf. Sci. Catal.* **1985**, *24*, 199–206.

(59) Thompson, R. W. *Zeolites* **1992**, *12*, 837–840.

goal of this study an interpretation might be put forward about the nature of species and bonding of the precursor short-range order assemblages preceding the nucleation process. On the basis of their localization and above depicted changes of the system a growth via changes of Si−O−Al bond angle and short-range transport of aluminosilicate species is the most plausible mechanism of formation. However, on the basis of the recent finding of Wakihara et al. one may expect that the four-member rings most probably dominate the nutrient pool providing species for zeolite A growth.[39]

Conclusions

Combined HP ^{129}Xe NMR−N_2 adsorption−HRTEM/EDS analyses, complemented by XRD, IR, SEM, and chemical analyses, were employed to shed light on the process of zeolite nucleation in sodium-rich aluminosilicate gels. The study can be recapitulated into two new findings: (i) the controlling effect of the concentration and diffusion rates of sodium on the polymerization and depolymerization reaction of aluminosilicate species and (ii) the critical role of interparticle voids in the nucleation process.

The obtained data shows that the concentration of alkali metal hydroxide in the initial system determines the size of the precursor gel particles. Namely, during the initial polymerization of the aluminosilicate precursor the concentration of sodium hydroxide in the solution increases; this restricts the extent of the polymerization process and leads to formation of small randomly aggregated gel particles with open structure. During the induction period a partial depolymerization takes place under the combined action of Na^+ and OH^-. Consequently, a chemical equilibrium between the solid and the liquid is reached, at which point the composition of the gel approaches the ultimate stoichiometric zeolite composition. It transpires that the onset of crystallization is controlled by two factors. First and well-known is the need that a critical mass of viable nuclei is produced. Second is the newly found requirement for a chemical evolution through diffusion that brings the gel to a homogeneous composition close to the zeolite stoichiometry before the crystallization starts.

Along with the chemical changes in the system substantial evolution of the gel structure is observed. A characteristic feature of sodium-rich aluminosilicate gel is the formation of cavities of mesopore dimensions, which disappear with the burst of crystallization reaction. The formation and development of these structures coincides temporally with the penetration of sodium into the bulk gel structure. The influence of the intraparticle voids formation on the process of zeolite A nucleation can be summarized as follows: (i) increase of the liquid−bulk gel interface, (ii) transport of nutrients through the gel network, (iii) creation of local saturations with compositions different from the bulk composition of the system, and (iv) transport of protozeolite nuclei to the bulk liquid.

As a consequence high nucleation rate is achieved, and the crystallization is completed within several hours. In contrast, for aluminosilicate systems with low alkali metal content much longer induction and crystallization periods are recorded due to low gel−solution interface for the bulk gel particles.

Besides issues related to fundamental aspects of zeolite crystallization the present study revealed the extremely high sensitivity of HP ^{129}Xe NMR in respect to microporous zeolite-type materials. Zeolite mass concentrations below 1 wt % of the total mass of the solid were unambiguously identified by the method.

Acknowledgment. V.V. acknowledges the financial support from the French−Croatia (COGITO) and French−Spanish (PICASSO) bilateral programs. W.Z. expresses thanks for the financial support of the National Natural Science Foundation of China (Grant No. 20873140) and the Ministry of Science and Technology of China (Grant No. 2009CB623507).

Supporting Information Available: IR spectra and SEM images of zeolite A and its precursors, chemical analysis of supernatant solutions, and local EDS analysis of gel particles. This material is available free of charge via the Internet at http://pubs.acs.org.

JA902088F